



# Memory effects of transcription regulator–DNA interactions in bacteria

Won Jung<sup>a,b,1</sup>, Tai-Yen Chen<sup>a,c</sup>, Ace George Santiago<sup>a,d</sup>, and Peng Chen<sup>a,1</sup>

Affiliations are included on p. 6.

Edited by Martin Gruebele, University of Illinois Urbana-Champaign, Urbana, IL; received April 20, 2024; accepted August 26, 2024

Memory effect refers to the phenomenon where past events influence a system's current and future states or behaviors. In biology, memory effects often arise from intra- or intermolecular interactions, leading to temporally correlated behaviors. Single-molecule studies have shown that enzymes and DNA-binding proteins can exhibit time-correlated behaviors of their activity. While memory effects are well documented and studied *in vitro*, no such examples exist in cells to our knowledge. Combining single-molecule tracking (SMT) and single-cell protein quantitation, we find in living *Escherichia coli* cells distinct temporal correlations in the binding/unbinding events on DNA by MerR- and Fur-family metalloregulators, manifesting as memory effects with timescales of ~1 s. These memory effects persist irrespective of the type of the metalloregulators or their metallation states. Moreover, these temporal correlations of metalloregulator–DNA interactions are associated with spatial confinements of the metalloregulators near their DNA binding sites, suggesting microdomains of ~100 nm in size that possibly result from the spatial organizations of the bacterial chromosome without the involvement of membranes. These microdomains likely facilitate repeated binding events, enhancing regulator–DNA contact frequency and potentially gene regulation efficiency. These findings provide unique insights into the spatiotemporal dynamics of protein–DNA interactions in bacterial cells, introducing the concept of microdomains as a crucial player in memory effect–driven gene regulation.

memory effects in protein–DNA interactions | microdomains in cells | gene regulation | MerR- and Fur-family regulators | single-molecule live-cell imaging

Memory effect refers to the phenomenon where past events influence a system's current and future states or behaviors (1). From an ecological perspective, the memory effect describes how an animal's past locations and movements influence its current trajectory and behavior (2–5). From the physical science point of view, the memory effect is often observed in ion channel kinetics, where the history of ion flow influences the channel's current state and function (6–12), in enzymes, which can exhibit time-correlated enzymatic turnover rates (13–20), and in nanoparticle catalysts, whose catalysis rates can also show temporal correlations like enzymes (21–24). In materials science, shape-memory alloys and polymers can remember their original shape and tend to return to their original states after deformation (25–30).

In biology, memory effects often arise from couplings of intra- or intermolecular interactions, in which a biological process, such as substrate binding or enzyme catalysis, affects another process a certain time later, leading to temporally correlated behaviors. Recent single-molecule enzymology studies have directly shown that the catalytic activity of a single enzyme molecule can fluctuate over time (a phenomenon also termed dynamic disorder) and show time-correlated behaviors (13–20, 31, 32). Single-molecule fluorescence imaging of the catalytic cycle of cholesterol oxidase is a classic example here, in which temporal memory of ~1 s was observed (13). These temporal memory effects are mechanistically linked to the underlying conformational dynamics that are coupled to the catalytic cycle at the enzyme active site (13–20, 31) and which could also give rise to bunching effects (32). Temporal memory was also observed in DNA-binding proteins. The rate-vs.-time of an individual  $\lambda$  exonuclease digesting double-stranded DNA exhibited a time correlation of ~145 s, suggesting the existence of dynamic disorder associated with conformational changes in the enzyme–DNA complex (16). Further, the nonequilibrium binding kinetics of the LexA repressor to DNA demonstrated a correlation with gene expression timing under various conditions of DNA damage during the SOS response (33).

While there is increasing evidence about memory effects in biology from *in vitro* experiments, no examples exist for such effects in cells to our knowledge. Whether protein

## Significance

Understanding transcriptional regulation in cells is critical to unraveling the complexities of gene expression. This study reports temporal memory effects in transcription regulator–DNA interactions in live bacterial cells. The identified ~1-s temporal correlations and ~100 nm spatial restrictions persist across multiple metal-responsive regulator types and their metallation states, suggesting a common cellular mechanism. The proposed model introduces the concept of cellular microdomains influencing gene regulation, providing insights into bacterial spatial organization and its functional implications. This work also extends the discussion of memory effects beyond *in vitro* studies, significantly contributing to the field of bacterial gene regulation.

Author contributions: W.J. designed research; W.J., T.-Y.C., and A.G.S. performed research; T.-Y.C. and A.G.S. contributed new reagents/analytic tools; W.J. and P.C. analyzed data; T.-Y.C. contributed to experiments; A.G.S. contributed to experiments; P.C. directed research; and W.J. and P.C. wrote the paper.

The authors declare no competing interest.

This article is a PNAS Direct Submission.

Copyright © 2024 the Author(s). Published by PNAS. This article is distributed under Creative Commons Attribution-NonCommercial-NoDerivatives License 4.0 (CC BY-NC-ND).

<sup>1</sup>To whom correspondence may be addressed. Email: won\_jung@fas.harvard.edu or pc252@cornell.edu.

This article contains supporting information online at <https://www.pnas.org/lookup/suppl/doi:10.1073/pnas.2407647121/-/DCSupplemental>.

Published October 3, 2024.

binding-unbinding on DNA can be affected by previous protein binding-unbinding in a cell is not known. Using single-molecule tracking (SMT) measurements, we recently studied the interactions of two families of metalloregulators with DNA in live *Escherichia coli* cells (34, 35); these metalloregulators help the cell maintain cellular metal homeostasis and defend against metal stress or depletion. One family is the MerR-family metal efflux regulators CueR and ZntR, which bind to their respective cognate sites on DNA either repressing (in their metal-free apo forms) or activating (in their respective  $\text{Cu}^+$  or  $\text{Zn}^{2+}$  bound holo forms) the transcription of metal efflux genes (36–39). The other is the Fur-family zinc uptake regulator Zur, which, in its fully metallated form, binds to its cognate sites on DNA repressing the transcription of zinc uptake genes (40–42); when its metal-sensing sites are vacant, Zur is a nonrepressor but can still bind to DNA tightly at nonconsensus sequence sites (35). SMT of these metalloregulators allowed for measuring their mobility, reflecting whether the protein molecule is freely diffusing in the cell or bound to DNA specifically or nonspecifically. We could resolve different mobility states and extract quantitative protein binding and unbinding kinetics to their tight binding sites on DNA.

In consideration of memory effects found in vitro, we explored the potential existence of related phenomena in metalloregulator–DNA interactions in bacterial cells. Here, we report the finding of memory effects in both binding to and unbinding from DNA in live *E. coli* cells for three metalloregulators: CueR, ZntR, and Zur. Such memory effects of metalloregulator–DNA binding/unbinding occur regardless of the type of the metalloregulator and of their metallation states. They also show comparable timescales of  $\sim 1$  s and are all associated with spatial restrictions of the

metalloregulator protein near DNA binding sites in the cell. These results led to our proposed model of protein diffusion confinement within microdomains of approximately  $\sim 100$  nm in size inside cells, possibly reflecting the spatial organizations of the bacterial chromosome without the involvement of membranes, which would be consistent with previously reported spatial organization of RNA polymerase in bacteria (43) and can provide functional advantages in gene regulation.

## Results and Analysis

**Temporal Correlations of Regulator Binding to DNA in Cells.** To perform SMT to identify binding of a regulator to DNA (i.e., chromosome) in cells, we fused the photoconvertible fluorescent protein mEos3.2 (44) to its C-terminus (i.e., creating CueR<sup>mE</sup>, ZntR<sup>mE</sup>, and Zur<sup>mE</sup>), either at its chromosomal locus to have physiological expression or additionally in an inducible plasmid to access a wider range of cellular protein concentrations (34, 35). With controlled photoconversion and time-lapse stroboscopic imaging, we obtained position trajectories of many individual proteins in single *E. coli* cells at tens of nanometer precision until their mEos3.2 tags photobleached (Fig. 1 *A*, *Inset*) (*SI Appendix, section 1*). We determined their cumulative distribution functions (CDFs) and probability density functions (PDFs) of displacement length  $r$  between subsequent images to quantify the diffusivity of individual proteins in a cell, as well as their respective fractional populations (Fig. 1*A*). In combination with control experiments including tracking the free mEos3.2 protein, we resolved the three diffusion states: the fastest diffusing state is assignable as those freely diffusing (FD) in the cytoplasm, the medium diffusion

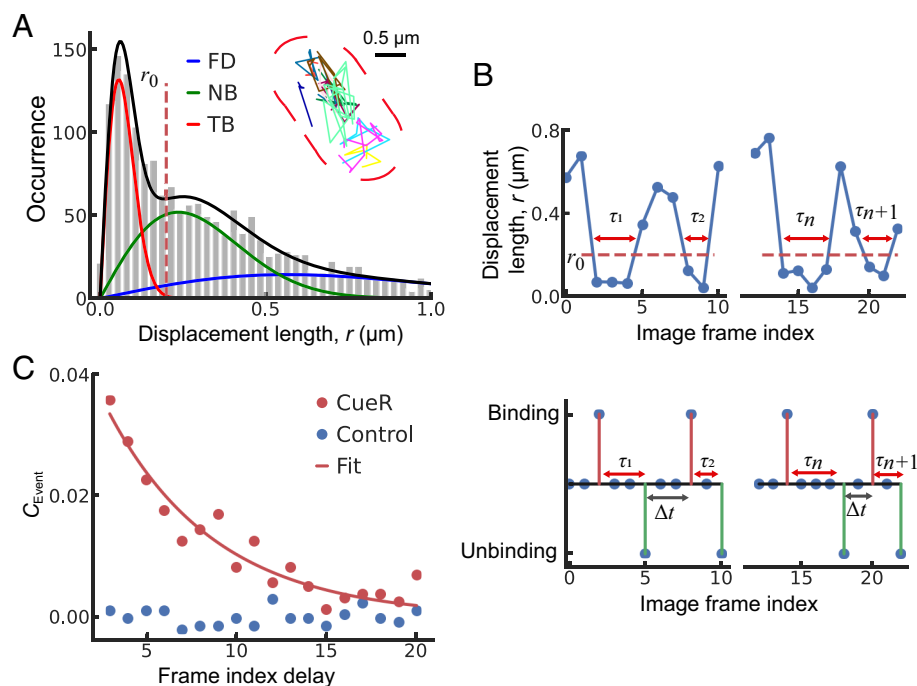


**Fig. 1.** Temporal correlations of regulator binding to DNA in living bacterial cells. (*A*) Distribution of displacement length  $r$  per time-lapse (60 ms) of >1,700 tracked CueR<sup>mE</sup> proteins at  $272 \pm 38$  nM CueR<sup>mE</sup> in the cell (the  $\pm$ error here refers to the SD among individual cells in this cellular protein concentration group). Solid lines: the overall fitted distribution (black), and FD (blue), NB (green), and TB (red) diffusion states with extracted effective diffusion constants of  $D_{\text{FD}} = 3.7 \pm 0.2$ ,  $D_{\text{NB}} = 0.56 \pm 0.03$ ,  $D_{\text{TB}} = 0.028 \pm 0.009 \mu\text{m}^2 \text{s}^{-1}$ , and the three states' fractional populations of  $A_{\text{FD}} = 26.1 \pm 0.2$ ,  $A_{\text{NB}} = 48.1 \pm 0.3$ ,  $A_{\text{TB}} = 25.8 \pm 0.3\%$  as defined in *SI Appendix, Eq. S1*. Vertical dashed line: threshold  $r_0 = 0.22 \mu\text{m}$  for extracting residence times in  $r$ -vs-time trajectories. *Inset*: Exemplary tracking trajectories of single CueR<sup>mE</sup> proteins (colored lines) in a live cell; dashed red line: cell outer contour. (*B*) *Top*: Exemplary time trajectories of displacement length  $r$  per time-lapse of single CueR<sup>mE</sup> proteins in a single cell.  $\tau_n$ 's are the microscopic residence times thresholded by  $r_0$  (red dashed line). The break in the x-axis denotes frame index separation. After the break, it shows the trajectory of another protein in the same cell. *Bottom*: corresponding assigned regulator binding (red vertical lines) and unbinding events on DNA (green vertical lines). (*C*) Autocorrelation function  $C_{\text{Event}}$  of the binding event sequence of CueR<sup>mE</sup> proteins (red) as in *B*, *Bottom*, and that of the corresponding randomized binding event sequence as a control (blue). The data are averaged over >1,700 tracked proteins from the condition as in *A*. Red line: exponential fit with a time constant of  $8 \pm 3$  in units of frame index, corresponding to  $0.5 \pm 0.2$  s (the  $\pm$ error here is 95% confidence bounds from the fit).

state as those nonspecifically bound (NB) to and moving on chromosome, and the slowest state as those tightly bound (TB) to the chromosome (e.g., at a recognition site) (Fig. 1A) (34, 35). We then used a whole-cell fluorescence-based protocol to quantify the remaining number of regulator molecules in the same cell, eventually determining the total protein concentration in each cell (34, 35). Protein–DNA interaction dynamics were examined by displacement-vs-time trajectories (Fig. 1B, Top). These trajectories show clear transitions between large and small  $r$  values. We set an upper threshold  $r_0$  (= 220 nm for CueR and ZntR and 200 nm for Zur), below which >99.5% of the TB states are included based on the resolved distributions of  $r$  (Fig. 1A). This  $r_0$ -thresholding of  $r$ -vs-time trajectories allows for the extraction of the approximate timing of binding and unbinding events of a regulator protein at a tight-binding site (i.e., transitions across the  $r_0$ -threshold; Fig. 1B, Bottom) as well as the estimate of the regulator protein's individual residence time  $\tau$  at that site (Fig. 1B, Top and Bottom).

To probe potential memory effects of regulators binding to DNA, we first examined the individual binding events in a single cell over a period of time (Fig. 1B, Bottom, upward red lines). Intriguingly, the sequence of binding events appeared to be bunched into clusters, as reflected by the autocorrelation function of the binding event sequence (Fig. 1C, red points). Specifically, at any cellular protein concentration, this autocorrelation function of the binding event sequence shows a positive amplitude and decays exponentially with increasing time delay (i.e., delay in image frame index, *SI Appendix, section 2.1*), indicating a temporal memory (e.g., Fig. 1C, red points, for CueR at a cellular protein concentration of ~272 nM; and *SI Appendix, Fig. S2* for other cellular concentrations of CueR, ZntR, and Zur). For CueR, the memory time is ~0.5 s, deduced from the exponential time constant (Fig. 1C, red line). This timescale is shorter than our photoconversion-imaging cycle time (1.8 s), indicating that it is likely the same protein rebinding to DNA within a single photoconversion and imaging cycle. Moreover, when the detected binding events are artificially randomized in time, such autocorrelation behavior vanishes (Fig. 1C, blue points), indicating that such autocorrelations stem from the inherent temporal arrangements of regulator binding events to DNA in the cell. Similar temporal memory effects of regulator binding to DNA were observed for CueR regardless of its metallation state as well as for ZntR and Zur (*SI Appendix, Fig. S2*). As CueR/ZntR and Zur belong to two distinct families of metal-responsive regulators and operate via different mechanisms for transcription regulation, such shared temporal memory effects of regulator binding to DNA should therefore stem more likely from some common cellular properties instead of properties specific to each protein.

**Temporal Correlation of Regulator Unbinding from DNA.** We then examined the temporal correlation of regulator unbinding events in individual cells (Fig. 1B, Bottom, downward green lines). To do so, we obtained the sequence of the residence time  $\tau_n$  in each cell ( $n$  is the event index; Fig. 1B), where the residence time  $\tau_n$  contains the unbinding kinetics of regulator from a DNA binding site. Each of such single-cell sequences contains the contributions from many individual regulator proteins observed over the many photoconversion/imaging cycles. We computed the autocorrelation function  $C_r(n)$  of the residence time sequence (*SI Appendix, section 2.2*). Once averaged over many such single-cell sequences to increase statistical significance, this autocorrelation function clearly shows a temporal memory: It has an initial positive amplitude and then decays exponentially with increasing delay index (e.g., Fig. 2A, red points, for CueR in cells having  $[\text{CueR}]_{\text{cell}} \sim 272$  nM). Randomization of the residence time

sequences abolishes such autocorrelation behaviors (Fig. 2A, blue points), indicating that such temporal correlations indeed stem from the temporal relations of the individual regulator unbinding events in the cell. The memory time constant of  $C_r(n)$  is  $\sim 5 \pm 4$  in terms of event index for CueR, comparable to the number of unbinding events observed in one photoconversion/imaging cycle that ranges from about 1 to 9 [averaging at  $2.4 \pm 0.8$  (SD)] and thus reflecting that this temporal memory originated mostly from the unbinding of the same CueR molecule that binds/unbinds multiple times on DNA in each photoconversion/imaging cycle. With the average spacing being  $\sim 0.27$  s between adjacent unbinding events within each imaging cycle, this temporal memory corresponds to  $\sim 1$  s. This timescale is comparable to the memory time ( $\sim 0.5$  s) of CueR's binding events in Fig. 1C and suggests that the temporal correlations of CueR binding and unbinding share similar underlying origins.

To directly represent the overall correlation strength, we averaged the correlation values of first eight delay indices (i.e.,  $\langle C_8 \rangle$ ) of the autocorrelation function  $C_r(n)$  of the residence time sequences; here, we did not use the amplitude of the exponential fit of the autocorrelation function because of its larger error bars. Expectedly,  $\langle C_8 \rangle$  decreases with increasing cellular CueR concentrations (Fig. 2A, inset), since at higher protein concentrations, more proteins competed for the limited number of binding sites on DNA, leading to smaller probability for the same regulator molecule to rebind to the same DNA site and thus dissipation of the memory effect. On the other hand, the temporal memory time of CueR unbinding is  $\sim 1$  s and has no significant dependence on  $[\text{CueR}]_{\text{cell}}$  (Fig. 2B, red points). Similar behaviors were observed for CueR regardless of its metallation state in the cell (Fig. 2B, green and blue points) as well as for ZntR and Zur at different metallation states (*SI Appendix, Fig. S3*), again supporting that such temporal memory effects stem more likely from some common cellular properties instead of properties specific to each protein.

Since the memory time suggests that the correlations of regulator unbinding likely results from the same protein molecule, we examined the temporally subsequent residence times  $\tau_1^i$  and  $\tau_2^i$  within the same  $i$ th photoconversion/imaging cycle. The  $\tau_1^i$  vs  $\tau_2^i$  of CueR at any cellular protein concentration shows a clear positive Pearson's cross correlation coefficient  $\rho$  (Fig. 2C), and this correlation coefficient decreases with increasing cellular protein concentrations (Fig. 2E). This trend persists regardless of CueR's metallation states (Fig. 2E) and of which regulator protein is examined (e.g., ZntR or Zur; *SI Appendix, Fig. S4*). As controls, randomizing  $\tau_2$  abolishes such correlation behaviors, and simulated random sequences of residence times do not show such correlations either (*SI Appendix, Fig. S5*).

One possible scenario to explain the diminished  $\tau_1^i$ – $\tau_2^i$  correlation at higher  $[\text{CueR}]_{\text{cell}}$  could be the increased competition for DNA binding sites. At higher cellular protein concentration, a single regular protein will take longer time to find a vacant DNA binding site and its probability to rebind to the same site would dissipate. To confirm this scenario, we sorted the  $\tau_1^i$ – $\tau_2^i$  pairs into four groups based on their time gap (i.e., the time separation  $\Delta t$  between  $\tau_1^i$  and  $\tau_2^i$ ; Fig. 1B, Bottom). For CueR,  $\tau_1^i$ – $\tau_2^i$  at any time gap also shows a positive correlation coefficient (Fig. 2D), which decreases exponentially with increasing time gaps (Fig. 2F), validating the scenario of memory dissipation with time. The exponential time constant here is  $\sim 1$  s (Fig. 2F), again similar to the timescale obtained from the autocorrelation functions of binding events (Fig. 1C) and residence time sequences (Fig. 2A and B).

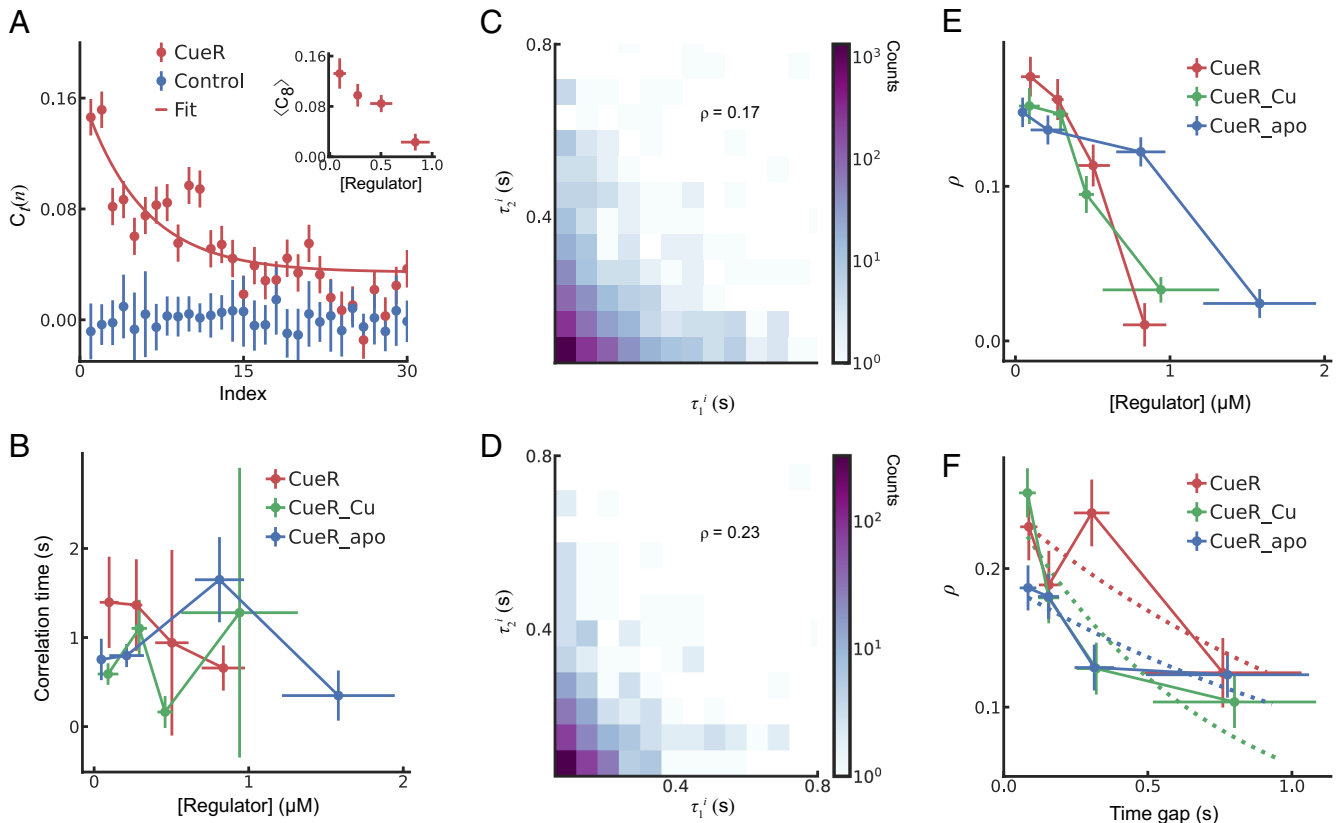


**Fig. 2.** Temporal correlation of regulator unbinding from DNA in living bacterial cells. (A) Event-based autocorrelation function  $C_A(n)$  of the residence time  $\tau$  sequence for CueR<sup>ME</sup> (red) from the condition as in Fig. 1A and that of the corresponding randomized residence time event sequence (blue). Red line: exponential fit with time constant of  $5 \pm 4$  in event index (the  $\pm$  error here is 95% confidence bounds from the fit). *Inset*: The average of the first eight points of the autocorrelation function  $C_A(n)$  vs. CueR<sup>ME</sup> concentration in the cell. (B) Dependence of autocorrelation time vs. CueR concentration in the cell at different CueR metallation states, as obtained from exponential fits in (A). Red: CueR; green: CueR<sup>ME</sup><sub>Cu</sub>; and blue: CueR<sup>ME</sup><sub>apo</sub>. (C) 2D histogram of regulator protein residence time  $\tau_1^i$  and the subsequent residence time  $\tau_2^i$  in the  $i$ th-photoconversion/imaging cycle for CueR at  $272 \pm 38$  nM. (D) 2D histogram of protein residence time  $\tau_1^i$  and the subsequent residence time  $\tau_2^i$  for CueR at an average time gap  $\Delta t$  of  $87 \pm 30$  ms. (E) Dependence of the Pearson's cross correlation coefficient  $\rho$  from C vs. regulator concentration in the cell at different regulator metallation states. (F) Dependence of Pearson's cross correlation coefficient  $\rho$  from D vs. average time gap  $\Delta t$  between subsequent unbinding events at different CueR metallation states. Dotted lines: exponential fits.

**Spatial Extent of Temporally Correlated Protein Binding/Unbinding on DNA Suggests the Existence of Cellular Microdomains.** The observed temporal correlations of protein binding to and unbinding from DNA in cells suggest that these correlations likely result from a regulator molecule binds to and unbinds from the same binding site on DNA, repetitively, during the associated memory time before the regulator diffuses away and samples other binding sites. We hypothesized that such repetitive regulator binding/unbinding on the same DNA site should come from some type of “microdomains” inside the cell, which temporarily confine a regulator molecule in the vicinity of a binding site on DNA, rendering the regulator more probable to rebound to the same binding site (Fig. 3, shaded area).

To probe whether such cellular microdomains exist and what their physical dimensions are, we analyzed a regulator's flight distance (i.e., the distance it traveled) while it is diffusing in the cell between two temporally neighboring binding events (Fig. 4A, *Inset*). If microdomains exist, a regulator should be more prone to exhibit short flight distances, rendered by the temporary confinement by the microdomains. This tendency of more frequent short flight distances is indeed evident in the histogram of CueR's flight distances (Fig. 4A)—While the histogram is satisfactorily fitted by an exponential distribution from the second bin toward longer flight distances (red line in Fig. 4A), the histogram's first bin is significantly greater than the expected value from the exponential fit, where the difference [i.e.,  $\Delta(\text{first bin})$ ] reflects the higher probability of shorter flight distances (e.g.,  $<380$  nm)

expected from the microdomain effect (*SI Appendix, section 2.3* for simulation validation that in the absence of microdomain effect, such flight distance distribution follows an apparent exponential distribution). Moreover, once sorting the cells into groups of similar CueR concentrations and analyze each group separately,  $\Delta(\text{first bin})$ , normalized by counts in the first bin, shows a decreasing trend with increasing cellular CueR concentration (Fig. 4B), consistent with that higher regulator concentrations lead to more competition of binding to the same site and higher probability of a particular regulator escaping the microdomain in search for other binding sites. Such behaviors are always observed regardless of CueR's metallation state (Fig. 4B) and are also observed for ZntR and Zur (*SI Appendix, Fig. S7*), supporting its being a general cellular phenomenon for DNA-binding proteins.

To better estimate the size of such microdomains, we further analyzed the distribution of pair-wise distances of all localizations along the flight distance between two sequential binding events (Fig. 4A, *Inset*) and compared it with that of two-dimensional projection of simulated three-dimensional random walk (*SI Appendix, section 2.4*). This pair-wise distance distribution for CueR has a peak at the shorter distance of  $\sim 100$  nm (Fig. 4C), while that of simulated random walk does not have such a peak (*SI Appendix, Fig. S9*). This peak at  $\sim 100$  nm therefore suggests that the microdomain that temporally confines the regulator during diffusion has an average diameter of  $\sim 100$  nm. Moreover, the fractional area of this peak at  $\sim 100$  nm in the distribution decreases when the cellular CueR concentration increases (Fig. 4D), consistent with

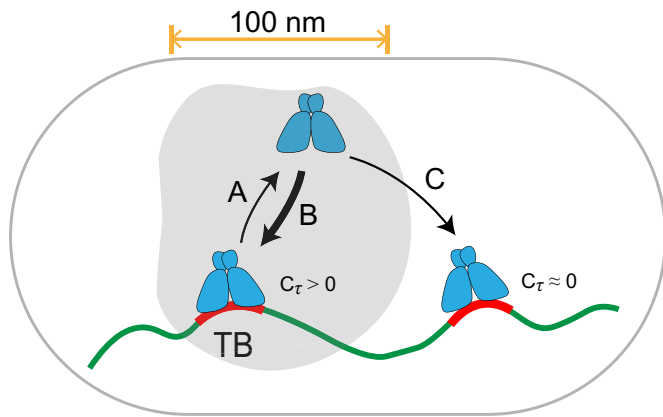


**Fig. 3.** Schematic representation of memory effect in regulators' binding/unbinding at DNA enabled by microdomains. (A) The initial unbinding of a metalloregulator from its tight binding site (TB, red) on chromosome (green). (B) The increased likelihood of a metalloregulator's rebinding to its original TB site within a microdomain (gray area). (C) The decreased tendency of metalloregulator binding to a TB site outside of the microdomain; in this context, protein's memory effect diminished gradually over time.

that a regulator is more probable to leave the microdomain owing to higher competition of rebinding to the same binding site within the microdomain. Such behaviors are again always observed regardless of CueR's metallation state (Fig. 4D) and are also observed for ZntR and Zur (SI Appendix, Fig. S8), consistent with that such microdomains are a cellular property affecting broadly the behaviors of DNA-binding proteins.

## Discussion

Here, we have uncovered temporal correlations of regulator binding and unbinding events on DNA in living *E. coli* cells that are associated with spatial restriction of the regulator protein near DNA-binding sites. The temporal correlation of  $\sim 1$  s and the spatial restriction of  $\sim 100$  nm both apply to three different metal-responsive transcription regulators and are independent of their being activators or repressors, all of which support the existence of microdomains within a bacterial cell (Fig. 3). What is the nature of these microdomains then? In contrast to eukaryotes, prokaryotes like bacteria are structurally simpler and do not have membrane-bound nucleus or organelles, leading to the simplistic perception of prokaryotes as simple entities in which proteins are floating freely in the cytoplasm. However, recent research has produced increasingly compelling evidence that bacterial cells exhibit a remarkable level of spatial organizations in their cellular components independent of membranes (45–48). For example, in *E. coli*, the 4.6 megabase pairs chromosome is organized into four structural macrodomains (Ori, Ter, Left, and Right chromosomal arms) and two unstructured regions, each consisting of small (average  $\sim 10$  kilobase pairs) topologically independent microdomains (49–51). The intracellular spatial organizations in bacteria may bear some analogies to micron-sized domains of phase separations, in which proteins and other biomacromolecules can form condensates (52–54). We postulate that such types of microdomains can exist around the chromosome (Fig. 3, shaded area), within which the DNA, including gene promoter regions, could be more

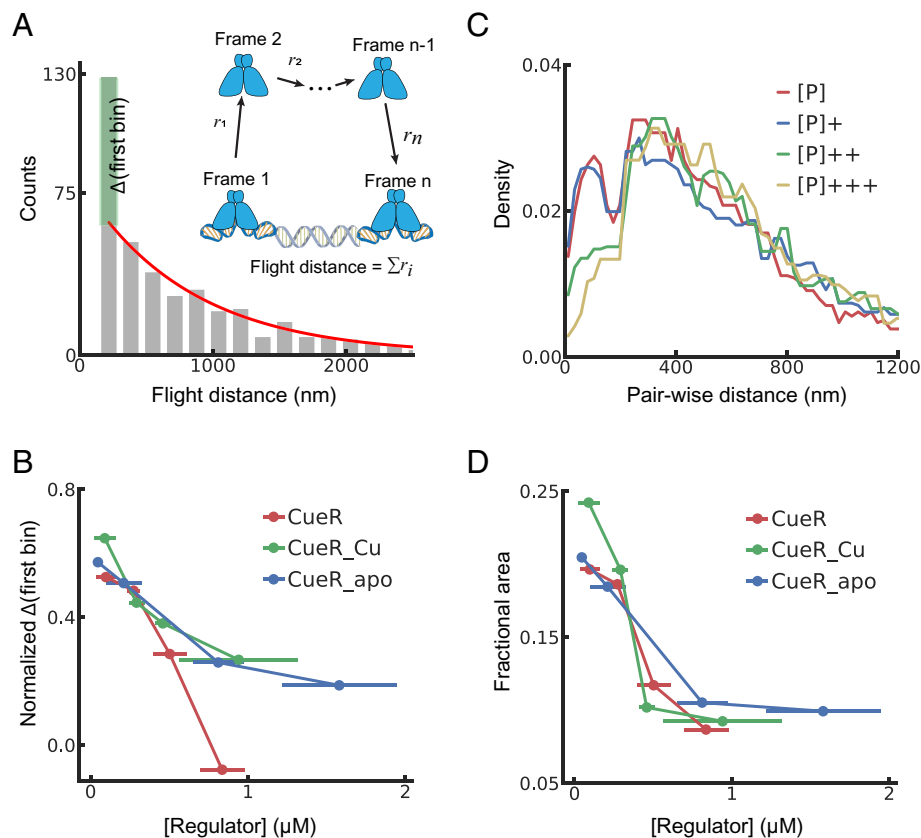


**Fig. 4.** Spatial range of temporally correlated protein binding and unbinding on DNA. (A) Histogram of flight distance for CueR between sequential binding events at  $[\text{CueR}^{\text{thE}}] = 97 \pm 61$  nM in the cell. Red line: exponential fit from the second bin. Green bar: difference between the first bin value and the expected value from the exponential fit [i.e.,  $\Delta(\text{first bin})$ ]. Inset: Schematic representation of a flight distance between two sequential binding events. (B)  $\Delta(\text{first bin})$  normalized by counts in the first bin vs. regulator concentration in the cell at different metallation states of CueR (red: CueR; green:  $\text{CueR}_{\text{Cu}}^{\text{mE}}$ ; and blue:  $\text{CueR}_{\text{apo}}^{\text{mE}}$ ). (C) Probability density distribution of pair-wise distance (PWD) for CueR along the flight distance at different regulator concentration in the cell [P]; red:  $[\text{CueR}] = 97 \pm 61$  nM; blue:  $[\text{CueR}] = 272 \pm 39$  nM; green:  $[\text{CueR}] = 503 \pm 108$  nM; yellow:  $[\text{CueR}] = 836 \pm 140$  nM. (D) The fractional area ( $A_{\text{PWD}<200}/A_{\text{all}}$ ) vs. regulator concentration in the cell for CueR at different metallation states.  $A_{\text{all}}$  is the area under the PWD density curve in C;  $A_{\text{PWD}<200}$  is the area up to pair-wise distance = 200 nm.

exposed to allow better access by proteins such as metalloregulators and give rise to the temporal correlations and spatial restrictions of metalloregulator–DNA interactions that we observed here. Relatedly, RNA polymerase in *E. coli* grown in rich medium has been shown to exhibit distinct spatial organizations, forming clusters of ~130 nm radius (43) that are comparable to the physical dimension of the microdomains we observed here.

These microdomains could possibly involve subcellular regions or compartments around transcription factor's DNA-binding sites and possess distinct physicochemical properties. These regions should be spatially separated from the surrounding cellular environment without hard boundaries like membranes and occupy a volume smaller than the entire cell. The differences in physicochemical properties within these microdomains may include variations in composition, such as specific proteins and DNA, and could perhaps be viewed as a different phase, such as phase-separated microdomains within the cytosol near the DNA-binding site. This phase separation could result from the chromosome behaving like long polymers with proteins specifically and nonspecifically bound to them. Recent chromosome conformation capture coupled with deep sequencing data and polymer modeling of the *Caulobacter crescentus* chromosome identified multiple, largely independent spatial domains that remain stable throughout the cell cycle (55); these domains are likely composed of supercoiled plectonemes arranged into a bottle brush-like fiber. Additionally, visualization of *E. coli* nucleoids reveals a dynamic helical ellipsoid structure demonstrating that nucleoid density coalesces into longitudinal bundles, forming a stiff, low-DNA-density ellipsoid confined radially within the cell (56). These longitudinal density fluctuations enhance internal nucleoid mobility and are involved in the cyclic accumulation and relief of intranucleoid mechanical stress, taken together suggesting that these subcellular domains are dynamic and regulated environments, which could be essential for transcription regulation.

Moreover, our measurement of metalloregulator–DNA interaction kinetics in the cell probes all possible DNA binding sites of these metalloregulators; these binding sites are located at many different locations in the *E. coli* genome (34, 35). Therefore, there should be a multitude of such microdomains in the cell, whose presence is likely dynamic because, in part, the chromosome conformation and organization are dynamic.

Functionally, the spatial restriction of metalloregulators within microdomains around DNA could potentially enhance regulator–DNA contact frequency by increasing the likelihood of regulator's rebinding to the same DNA site (i.e., enhancing step B and

suppressing step C in Fig. 3), effectively creating a transcription hotspot akin to those observed in eukaryotes (57). This spatial restriction effectively enables repressors or activators to remain associated with DNA (i.e., suppressing step C in Fig. 3) or to readily rebind to DNA (i.e., enhancing step B in Fig. 3), leading to more efficient repression or activation of their regulons. Moreover, this spatial restriction might also benefit sequence-recognizing proteins, facilitating their effective search for DNA targets within the microdomains (58–60). Therefore, microdomains could potentially play an important role in optimizing the interactions between sequence-recognizing proteins and DNA, thereby enhancing the efficiency of gene regulation within the cell.

## Materials and Methods

*Materials and Methods* are described in detail in *SI Appendix, section 1*. All constructed strains were derived from the *E. coli* BW25113 strain (CGSC# 7739 Keio Collection, Yale; genotype: (F<sup>-</sup>, Δ(*araD-araB*)567, Δ*lacZ*4787(::*rrnB-3*), λ<sup>-</sup>, *rph-1*, Δ(*rhaD-rhaB*)568, *hdsR514*)(*SI Appendix, section 1.1*). The lambda-red homologous recombination technique was used to construct the tagging of CueR, ZntR, and Zur with the photoconvertible fluorescent protein mEos3.2 (i.e., mE) at their respective chromosomal loci and the corresponding deletion strains. We previously confirmed the intactness and functionality of the mEos3.2-tagged proteins (34, 35). We also constructed the CueR<sup>mE</sup>, ZntR<sup>mE</sup>, and Zur<sup>mE</sup> gene fusions each in the L-arabinose-inducible plasmid pBAD24. The plasmids were each subsequently transformed into the strains of interests to have higher and controllable protein concentrations inside the cells. Site-directed mutagenesis using QuikChange mutagenesis kit (Stratagene) was employed to create mutant forms of CueR, ZntR, and Zur in the pBAD24 plasmid, which was then introduced into the cell in which the corresponding chromosomal copy of the gene was deleted. To prepare a sample for imaging, cells were grown overnight in LB with appropriate antibiotics, diluted in supplemented M9 medium, and then grown until OD<sub>600</sub> ~ 0.3 (*SI Appendix, section 1.2*). Imaging protocols included single-molecule imaging, tracking, and counting; and whole-cell fluorescence quantitation (*SI Appendix, section 1.2*). The displacement length distributions of tracked single-protein molecules were analyzed to quantify their diffusive behaviors, including the resolvable number of diffusion states, the effective diffusion constants, and their fractional populations (*SI Appendix, section 1.3*).

**Data, Materials, and Software Availability.** All study data are included in the article and/or *SI Appendix*.

**ACKNOWLEDGMENTS.** This research is supported by NIH Grant GM109993 (P.C.).

Author affiliations: <sup>a</sup>Department of Chemistry and Chemical Biology, Cornell University, Ithaca, NY 14853; <sup>b</sup>Department of Chemistry and Chemical Biology, Harvard University, Cambridge, MA 02138; <sup>c</sup>Department of Chemistry, University of Houston, Houston, TX 77204; and <sup>d</sup>10x Genomics, Pleasanton, CA 94588

1. J. Beran, Y. Feng, S. Ghosh, R. Kulik, "Definition of long memory", in *Long-Memory Processes: Probabilistic Properties and Statistical Methods*, J. Beran, Y. Feng, S. Ghosh, R. Kulik, Eds. (Springer Berlin Heidelberg, Berlin, Heidelberg, 2013), pp. 1–41.
2. P. M. Kareiva, N. Shigesada, Analyzing insect movement as a correlated random walk. *Oecologia* **56**, 234–238 (1983).
3. S. Dray, M. Royer-Carenzi, C. Calenge, The exploratory analysis of autocorrelation in animal-movement studies. *Ecol. Res.* **25**, 673–681 (2010).
4. B. T. McClintock, D. S. Johnson, M. B. Hooten, J. M. Ver Hoef, J. M. Morales, When to be discrete: The importance of time formulation in understanding animal movement. *Mov. Ecol.* **2**, 21 (2014).
5. E. Gurarie *et al.*, Correlated velocity models as a fundamental unit of animal movement: Synthesis and applications. *Mov. Ecol.* **5**, 13 (2017).
6. R. A. Nogueira, W. A. Varanda, L. S. Liebovitch, Hurst analysis in the study of ion channel kinetics. *Braz. J. Med. Biol. Res.* **28**, 491–496 (1995).
7. Z. Siwy, S. Mercik, K. Weron, M. Ausloos, Application of dwell-time series in studies of long-range correlation in single channel ion transport: Analysis of ion current through a big conductance locust potassium channel. *Phys. A-Stat. Mech. Appl.* **297**, 79–96 (2001).
8. Z. Siwy, M. Ausloos, K. Ivanova, Correlation studies of open and closed state fluctuations in an ion channel: Analysis of ion current through a large-conductance locust potassium channel. *Phys. Rev. E* **65**, 031907 (2002).
9. H. T. Bandeira, C. T. Barbosa, R. A. De Oliveira, J. F. Aguiar, R. A. Nogueira, Chaotic model and memory in single calcium-activated potassium channel kinetics. *Chaos* **18**, 033136 (2008).
10. I. M. de la Fuente *et al.*, Dynamic properties of calcium-activated chloride currents in *Xenopus laevis* oocytes. *Sci. Rep.* **7**, 41791 (2017).
11. A. Wawrzkiwicz-Jalowiecka, P. Trybek, L. Machura, B. Dworakowska, Z. J. Grzywna, Mechanosensitivity of the BK channels in human glioblastoma cells: Kinetics and dynamical complexity. *J. Membr. Biol.* **251**, 667–679 (2018).
12. M. P. Silva, C. G. Rodrigues, W. A. Varanda, R. A. Nogueira, Memory in ion channel kinetics. *Acta Biotheor.* **69**, 697–722 (2021).
13. H. P. Lu, L. Xun, X. S. Xie, Single-molecule enzymatic dynamics. *Science* **282**, 1877–1882 (1998).
14. J. S. Cao, Single molecule tracking of heterogeneous diffusion. *Phys. Rev. E* **63**, 041101 (2001).
15. S. L. Yang, J. S. Cao, Direct measurements of memory effects in single-molecule kinetics. *J. Chem. Phys.* **117**, 10996–11009 (2002).
16. A. M. Van Oijen *et al.*, Single-molecule kinetics of lambda exonuclease reveal base dependence and dynamic disorder. *Science* **301**, 1235–1238 (2003).
17. O. Flomenbom *et al.*, Stretched exponential decay and correlations in the catalytic activity of fluctuating single lipase molecules. *Proc. Natl. Acad. Sci. U.S.A.* **102**, 2368–2372 (2005).
18. B. P. English *et al.*, Ever-fluctuating single enzyme molecules: Michaelis-Menten equation revisited. *Nat. Chem. Biol.* **2**, 87–94 (2006).
19. G. De Cremer *et al.*, Dynamic disorder and stepwise deactivation in a chymotrypsin catalyzed hydrolysis reaction. *J. Am. Chem. Soc.* **129**, 15458–15459 (2007).
20. D. Zheng, H. P. Lu, Single-molecule enzymatic conformational dynamics: Spilling out the product molecules. *J. Phys. Chem. B* **118**, 9128–9140 (2014).

21. W. Xu, J. S. Kong, Y. T. Yeh, P. Chen, Single-molecule nanocatalysis reveals heterogeneous reaction pathways and catalytic dynamics. *Nat. Mater.* **7**, 992–996 (2008).
22. X. Zhou, W. Xu, G. Liu, D. Panda, P. Chen, Size-dependent catalytic activity and dynamics of gold nanoparticles at the single-molecule level. *J. Am. Chem. Soc.* **132**, 138–146 (2010).
23. K. S. Han, G. K. Liu, X. C. Zhou, R. E. Medina, P. Chen, How does a single Pt nanocatalyst behave in two different reactions? A single-molecule study. *Nano Lett.* **12**, 1253–1259 (2012).
24. Y. W. Zhang *et al.*, Superresolution fluorescence mapping of single-nanoparticle catalysts reveals spatiotemporal variations in surface reactivity. *Proc. Natl. Acad. Sci. U.S.A.* **112**, 8959–8964 (2015).
25. A. Lendlein, S. Kelch, Shape-memory polymers. *Angew. Chem. Int. Ed. Engl.* **41**, 2035–2057 (2002).
26. S. I. Gunes, S. C. Jana, Shape memory polymers and their nanocomposites: A review of science and technology of new multifunctional materials. *J. Nanosci. Nanotechnol.* **8**, 1616–1637 (2008).
27. D. C. Hofmann, Materials science. Shape memory bulk metallic glass composites. *Science* **329**, 1294–1295 (2010).
28. W. M. Huang *et al.*, Shaping tissue with shape memory materials. *Adv. Drug. Deliv. Rev.* **65**, 515–535 (2013).
29. A. Planes, L. Manosa, Shape-memory materials: Nanoscale oxides shape up. *Nat. Mater.* **13**, 6–8 (2014).
30. X. Z. Xin, L. W. Liu, Y. J. Liu, J. S. Leng, Mechanical models, structures, and applications of shape-memory polymers and their composites. *Acta. Mech. Solida. Sin.* **32**, 535–565 (2019).
31. H. P. Lerch, R. Rigler, A. S. Mikhailov, Functional conformational motions in the turnover cycle of cholesterol oxidase. *Proc. Natl. Acad. Sci. U.S.A.* **102**, 10807–10812 (2005).
32. H. P. Lu, Revealing time bunching effect in single-molecule enzyme conformational dynamics. *Phys. Chem. Chem. Phys.* **13**, 6734–6749 (2011).
33. M. J. Culyba, J. M. Kubiak, C. Y. Mo, M. Goulian, R. M. Kohli, Non-equilibrium repressor binding kinetics link DNA damage dose to transcriptional timing within the SOS gene network. *PLoS Genet.* **14**, e1007405 (2018).
34. T. Y. Chen *et al.*, Concentration- and chromosome-organization-dependent regulator unbinding from DNA for transcription regulation in living cells. *Nat. Commun.* **6**, 7445 (2015).
35. W. Jung, K. Sengupta, B. M. Wendel, J. D. Helmann, P. Chen, Biphasic unbinding of a metalloregulator from DNA for transcription (de)repression in Live Bacteria. *Nucleic Acids Res.* **48**, 2199–2208 (2020).
36. F. W. Outten, C. E. Outten, J. Hale, T. V. O'halloran, Transcriptional activation of an Escherichia coli copper efflux regulon by the chromosomal MerR homologue, cueR. *J. Biol. Chem.* **275**, 31024–31029 (2000).
37. C. E. Outten, T. V. O'halloran, Femtomolar sensitivity of metalloregulatory proteins controlling zinc homeostasis. *Science* **292**, 2488–2492 (2001).
38. S. Khan, K. R. Brocklehurst, G. W. Jones, A. P. Morby, The functional analysis of directed amino-acid alterations in ZntR from Escherichia coli. *Biochem. Biophys. Res. Commun.* **299**, 438–445 (2002).
39. A. Changela *et al.*, Molecular basis of metal-ion selectivity and zeptomolar sensitivity by CueR. *Science* **301**, 1383–1387 (2003).
40. E. M. Panina, A. A. Mironov, M. S. Gelfand, Comparative genomics of bacterial zinc regulons: Enhanced ion transport, pathogenesis, and rearrangement of ribosomal proteins. *Proc. Natl. Acad. Sci. U.S.A.* **100**, 9912–9917 (2003).
41. K. Hantke, Bacterial zinc uptake and regulators. *Curr. Opin. Microbiol.* **8**, 196–202 (2005).
42. B. A. Gilston *et al.*, Structural and mechanistic basis of zinc regulation across the E. coli Zur regulon. *PLoS Biol.* **12**, e1001987 (2014).
43. X. Weng *et al.*, Spatial organization of RNA polymerase and its relationship with transcription in Escherichia coli. *Proc. Natl. Acad. Sci. U.S.A.* **116**, 20115–20123 (2019).
44. M. Zhang *et al.*, Rational design of true monomeric and bright photoactivatable fluorescent proteins. *Nat. Methods* **9**, 727–729 (2012).
45. R. Losick, L. Shapiro, Changing views on the nature of the bacterial cell: From biochemistry to cytology. *J. Bacteriol.* **181**, 4143–4145 (1999).
46. L. Shapiro, H. H. Mcadams, R. Losick, Why and how bacteria localize proteins. *Science* **326**, 1225–1228 (2009).
47. X. Weng, J. Xiao, Spatial organization of transcription in bacterial cells. *Trends Genet.* **30**, 287–297 (2014).
48. B. R. Gilbert *et al.*, Dynamics of chromosome organization in a minimal bacterial cell. *Front Cell Dev. Biol.* **11**, 1214962 (2023).
49. L. Postow, C. D. Hardy, J. Arsuaga, N. R. Cozzarelli, Topological domain structure of the Escherichia coli chromosome. *Genes Dev.* **18**, 1766–1779 (2004).
50. F. Boccard, E. Esnault, M. Valens, Spatial arrangement and macrodomain organization of bacterial chromosomes. *Mol. Microbiol.* **57**, 9–16 (2005).
51. J. Holowka, J. Zakrzewska-Czerwinska, Nucleoid associated proteins: The small organizers that help to cope with stress. *Front Microbiol.* **11**, 590 (2020).
52. V. Yeong, E. G. Werth, L. M. Brown, A. C. Obermeyer, Formation of biomolecular condensates in bacteria by tuning protein electrostatics. *ACS Cent. Sci.* **6**, 2301–2310 (2020).
53. G. Munoz-Gil *et al.*, Stochastic particle unbinding modulates growth dynamics and size of transcription factor condensates in living cells. *Proc. Natl. Acad. Sci. U.S.A.* **119**, e2200667119 (2022).
54. B. Ramm *et al.*, Biomolecular condensate drives polymerization and bundling of the bacterial tubulin FtsZ to regulate cell division. *Nat. Commun.* **14**, 3825 (2023).
55. T. B. Le, M. V. Imakaev, L. A. Mirny, M. T. Laub, High-resolution mapping of the spatial organization of a bacterial chromosome. *Science* **342**, 731–734 (2013).
56. J. K. Fisher *et al.*, Four-dimensional imaging of E. coli nucleoid organization and dynamics in living cells. *Cell* **153**, 882–895 (2013).
57. C. Moorman *et al.*, Hotspots of transcription factor colocalization in the genome of Drosophila melanogaster. *Proc. Natl. Acad. Sci. U.S.A.* **103**, 12027–12032 (2006).
58. G. W. Li, O. G. Berg, J. Elf, Effects of macromolecular crowding and DNA looping on gene regulation kinetics. *Nat. Phys.* **5**, 294–297 (2009).
59. A. Mondal, A. Bhattacharjee, Searching target sites on DNA by proteins: Role of DNA dynamics under confinement. *Nucleic Acids Res.* **43**, 9176–9186 (2015).
60. M. Stracy *et al.*, Transient non-specific DNA binding dominates the target search of bacterial DNA-binding proteins. *Mol. Cell* **81**, 1499–1514 (2021).